Earth Surf. Dynam. Discuss., https://doi.org/10.5194/esurf-2018-85
Manuscript under review for journal Earth Surf. Dynam.
Discussion started: 18 December 2018

Modelling confluence dynamics in large sand-bed braided rivers

Haiyan Yang[1], Zhenhuan Liu[2]

[1]College of Water Conservancy and Civil Engineering, South China Agricultural University, Guangzhou 510642, China; haiyan.yang2@gmail.com

[2] Guangdong Provincial Key Laboratory of Urbanization and Geo-simulation, School of Geography and Planning, Sun Yat-sen University, Guangzhou 510275, China

Correspondence: liuzhh39@mail.sysu.edu.cn

Abstract

Confluences are key morphological nodes in braided rivers where flow converges, creating complex flow patterns and rapid bed deformation. Field survey and laboratory experimental studies have been carried out to investigate the morphodynamic features in individual confluences, but few have investigated the evolution process of confluences in large braided rivers. In the current study a physics-based numerical model was applied to simulate a large lowland braided river dominated by suspended sediment transport, and analyzed the morphologic changes at confluences and their controlling factors. It was found that the confluences in large braided rivers exhibit some dynamic processes and geometric characteristics that are similar to those observed in individual confluences arising from two tributaries. However, they also show some unique characteristics that are result from the influence of the overall braided pattern and especially of neighboring upstream channels.

Key words: braided river, numerical model, confluence, dynamics, geometry, scour hole

1. Introduction

Braided rivers are highly dynamic systems characterized by multiple frequently joining and bifurcating channels that form confluences and bifurcations. In these rivers, channel confluences and bifurcations are key morphological features whose dynamics and mutual interactions control many aspects of channel morphology and processes in braided networks. Exploring the mechanisms underlying confluence evolution is fundamental to better understand morphodynamic processes in braided rivers (Surian, 2015). Confluences as the junctions of two river branches have been widely studied both in field (e.g., Rhoads et al. 2009; Riley et al., 2015) and in laboratory (e.g., Ribeiro et al., 2012; Guillén-Ludeña et al., 2016), with a few focusing on large-scale confluences (e.g., Szupiany et al., 2009; Gualtieri et al., 2018). However, confluences in large braided rivers have rarely been investigated, mainly due to the lack of adequate methodologies to investigate large rivers with frequent channel migrations. The evolution and morphology of confluences in large braided rivers share some common features with junctions of two branches in a non-braided river. However, they might also be affected by the evolution of the overall braided pattern, especially by morphologic changes in their immediate upstream neighbourhood, thereby exhibiting unique morphodynamic processes and characteristics.

Channel confluences are important sites where adjustments in flow structure, sediment transport and channel morphology occur to accommodate convergence of water and sediment from different branches (Ferguson et al., 1992; Rhoads et al., 2009). Common morphologic features often include a scour hole typically oriented along the direction of maximum velocity, avalanche faces at the mouth of each branch, sediment deposition within the stagnation zone at the upstream junction corner, and bars formed within the flow separation zone (Rhoads and Kenworthy, 1995, 1998; Best and Rhoads, 2008). The main factors that control flow structure and channel morphology at confluences include flow and sediment discharge ratios between the two confluent channels, the confluence angle and its planform asymmetry, and the degree of bed concordance between the confluent channels (e.g. Szupiany et al., 2009). Recent findings indicate that bifurcation asymmetry is not solely controlled by flow discharge but is rather the result of multiple factors, including varying flow discharge, changes in bed morphology and cross-stream water surface slopes (Gualtieri et al., 2018). Guillén-Ludeña et al. (2016) found that the abundant sediment load of the dominant branch plays a major role in controlling the dynamics of mountain river confluences.

The center of a confluence often features a scour hole with considerable erosion depth. The scour zone may change from trough-shaped to more basin-like as the confluence angle increases (Ashmore and Parker, 1983; Best, 1986). The scour depth of a confluence has been related to the confluence angle and the relative discharge of the confluent channels (e.g., Best, 1988), which typically ranges from two to four times the incoming branch channel depths, suggesting some scale invariance in junction morphology (Parsons et al., 2008). The slopes of beds dipping into scour holes in large braided rivers are often gentle, e.g., less than 5% in the Brahamaputra River (Best and Ashworth, 1997).

Numerical models are useful tools to assist field research because they can provide large datasets with sufficient spatial and temporal resolution to investigate river morphodynamics. In recent years, numerical models based on the basic flow and sediment transport equations, such as the depth-integrated Delft 3-D (Schuurman et al., 2013; Schuurman and Kleinhans, 2015), HSTAR (Nicholas, 2013) and other models (e.g., Jang and Shimizu, 2005a, b; Yang, 2013) have been developed and applied to simulate braided rivers. These models provided new insights into the dynamic processes of braided rivers and enriched theories for these systems. Yang et al. (2015, 2018) developed a 2-D physics-based model that divides sediment into multiple fractions and riverbed into several vertical layers, and simulated rivers with morphodynamics compared well with natural braided rivers. They analysed the dynamic processes and statistical features in these rivers and investigated the key factors controlling channel generation and disappearance.

The present paper applies that model (Yang et al., 2015, 2018) to simulate large lowland sand-bed braided reaches. The main objectives of the study are to quantitatively analyse changes in flow field, sediment concentration and bed elevation at typical confluences, compare them with those observed in natural rivers, and investigate evolution processes at confluences and the controlling factors. Results of this study will expand the current knowledge on confluence dynamics in large sand-bed braided rivers and provide the opportunity to analyse similarities and differences between braided rivers and other river types.

2. Model Descriptions and Methods

2.1 Numerical model and solutions

A two-dimensional depth-integrated numerical model was applied to simulate the confluence dynamics in the lower reaches of large sand-bed braided rivers. The hydrodynamic model consists of a mass and two momentum conservation equations, which are derived from the three-dimensional Reynolds equations for incompressible and unsteady turbulent flows by depth integrated. The hydrodynamic equations are solved using the Alternating Direction Implicit method, which has been widely used in the solution of shallow water equations (e.g. Lin and Falconer, 2006).

The sediment transport is described by a two-dimensional solute transport equation and a bed deformation equation, with a fractional method adopted to simulate the sorting process of graded sediments. By dividing the graded sediments into N fractions, the transport of the kth size fraction is calculated by

$$\frac{\partial Hs_k}{\partial t}+\frac{\partial HUs_k}{\partial x}+\frac{\partial HVs_k}{\partial y}=-\alpha_k\omega_k\left(s_k-\phi_k\right)+\frac{\partial}{\partial x}\left(D_{xx}H\frac{\partial s_k}{\partial x}+D_{xy}H\frac{\partial s_k}{\partial y}\right)+\frac{\partial}{\partial y}\left(D_{yx}H\frac{\partial s_k}{\partial x}+D_{yy}H\frac{\partial s_k}{\partial y}\right) \tag{4}$$

The riverbed deformation is given as

$$\left(1-p_0\right)\frac{\partial z_b}{\partial t}=\frac{1}{\gamma_s}\sum\alpha_k\omega_k\left(s_k-\phi_k\right) \tag{5}$$

where s_k is the sediment concentration for size fraction k; α_k is the adjustment coefficient for size fraction k; ω_k is the fall velocity for size fraction k, calculated by the equation of van Rijn (1984); ϕ_k is the transport capacity for size fraction k; D_{xx}, D_{xy}, D_{yx} and D_{yy}

are depth-averaged dispersion–diffusion coefficients in the x and y directions, respectively, with Preston's (1985) equations adopted; p_0 is the porosity of bed layer sediments; z_b is the riverbed elevation; and γ_s is the specific weight of sediment.

In order to account for the influence of bed composition, a multiple layer method is used to simulate the spatial and temporal variations of sediment gradations in the loose bed layers. The sediment transport equations were solved with the Ultimate QUICKEST Scheme, which was developed to simulate 2-D solute and mass transport with high concentration gradients (Lin and Falconer, 1997). More details on the model and solution method can be found in Yang (2013), Yang et al (2015), Zhou et al (2003), and Zhou and Lin (2006).

2.2 Model settings and boundary conditions

The model was set up based on the data collected from the lower reaches of Jiahetan and Huayuankou in the Yellow River in China (Zhao et al. 1998; Wu 2007), including flow discharge, bed slope, sediment size distribution and channel dimension. The simulated river was approximately 50 km long and 5 km wide, initially straight and plane, with a uniform bed slope of 0.000233. The model divided the sediments into six fractions, with particle sizes ranging from 0.0025 to 0.25 mm. Two spur dikes were set up at the right and left bank near the upstream boundary to increase the local flow speed, aiming to accelerate the initial channel evolution process. The input flow discharge was given as 6250 m^3/s, and the sediment concentration was set to 44.5 kg/m^3 referred to the field data of the Yellow River.

3. Channel Confluences

3.1 General processes

Instabilities in the simulated braided river were initiated in the alternate shallow and deep areas near the upstream spurs. This induced flow disturbance and caused intense erosion and deposition in the neighbouring areas and subsequently downstream (Figure 1). A braided pattern was then formed through the development of multiple row bars, which is one of the two most common mechanisms of braided pattern evolution in rivers (Ashmore, 2009). Channels divided and rejoined around bars, forming nodes typical in braided rivers—confluences and bifurcations, usually with deep scour holes in their center.

<Figure 1 insert here>

Figure 1 Sequential evolution of confluences in the modelled river (water depth/m)

One confluence and its upstream bifurcation, with the two converging branches and their surrounding bar, form a pool-bar unit, the basic element of a braided river. The confluence of a pool-bar unit is simultaneously the bifurcation of another pool-bar unit and also represents the branch bend scouring pool of a third confluence. For example, confluence D is the scouring pool of the right branch of confluence E in Figure 1. Nodes can also evolve and change their roles. For example, the scouring pool at the outer bank of two branches of a confluence can travel downstream to renew the confluence. This is what happened to pool 1 (day 26 in Figure 1), which continued

Earth Surf. Dynam. Discuss., https://doi.org/10.5194/esurf-2018-85
Manuscript under review for journal Earth Surf. Dynam.
Discussion started: 18 December 2018

extending downstream and merged with confluence C on day 33. Confluences can also migrate downstream. High flow can cause fine sediment erosion at a bifurcation and at the two front sides of its downstream bar head, with subsequent transport of the eroded sediments downstream and deposition at the bar-tail confluence, thereby causing infilling of the confluence head and scouring of the confluence tail. One example of this mechanism is shown by confluence E. Downstream movement of a confluence is also common in natural rivers and has been suggested to be controlled by aggradation in the confluence area and local avulsions of the primary channel (Roy and Sinha, 2007).

The pool in the dominant branch of a confluence often developed at the front of the channel bend and featured a substantial scouring depth (e.g., pool 1 in Figure 1). Conversely, the pool in the secondary branch tended to develop behind the channel bend and was characterized by a relatively shallow scouring depth (e.g., pool 2 in Figure 1). However, sometimes in a thin pool-bar unit formed in the early stage, the scouring pools of both branches developed at the front of the channel bend. One example is pool-bar unit 3 in Figure 1 on day 26. As the bar grew laterally and shortened, the pool migrated downstream across the bend.

3.2 Geometry and controlling factors

Confluences are normally located in areas with deepest flow due to the fact that where two or more branches meet intense erosion occurs, thereby removing a large amount of sediments. Figure 2 shows the cross-sectional maximum erosion depth compared to river geometry in a fully evolved braided river, with A–G indicating the location of typical confluences both in the river and along the corresponding erosion

Earth Surf. Dynam. Discuss., https://doi.org/10.5194/esurf-2018-85
Manuscript under review for journal Earth Surf. Dynam.
Discussion started: 18 December 2018

curve. The maximum erosion depth curve exhibits a periodic wave pattern with peaks and valleys, representing local minimum and maximum erosion depths, respectively. Generally, most of the cross-sectional topographic valleys are located at confluences, while the remaining valleys are often scouring pools at channel bends between two confluences. Confluence erosion tends to be more intense when the total confluence channel width is narrower.

<Figure 2 insert here>

Figure 2 Cross-sectional maximum erosion depth compared to river geometry in a fully evolved river (day 33)

Table 1 Parameters of seven typical confluences in a fully evolved river (day 33)

<Table 1 insert here>

Table 1 lists the gross hydraulic and geometric features of confluences A–G. The deepest scour hole mostly occurred at the confluences with two branches most similar to each other. For example, despite not having the fastest flow or largest discharge, confluence E (discharge ratio being 1.16, closest to 1) still developed the deepest scour hole (4.01 m). Nevertheless, the confluence with branches least similar to each other (e.g. discharge ratio being 3.27 for confluence A) also formed a remarkably deep scour hole (3.99 m), when the dominant branch played a key role in this process.

The angle between the two branches of the simulated confluences increased with decreasing discharge ratio, while it was also influenced by the morphological changes in surrounding areas, especially by upstream channel evolution. For example, with the lowest discharge ratio, the two branches of confluence E developed a larger confluence angle than most of the other confluences. However, confluence F had relatively high discharge ratio but developed the largest branch angles, too. This might be due to the fact that the flow direction of the secondary branch (left branch for confluence F) was largely determined by the flow of its upstream bifurcation.

The confluence scour axis tends to parallel the dominant branch, which has been observed in laboratory experiments (e.g. Ashmore and Parker, 1983; Best, 1987), forming a smaller angle with it, with the exception of confluences C and G. On one hand, faster flow existing in the dominant branch eroded more sediments from the riverbed and formed the scour hole head. On the other hand, the flow direction of a confluence oriented towards the dominant branch, determining the scour hole axis direction. However, at confluences C and G, the confluence scour axis was directed towards the secondary branch. For confluence C, the scour hole intruded into the secondary (left) branch (Figure 3a), so that the hole direction was mainly determined by the secondary branch flow. For confluence G, flow was influenced by upstream channel evolution and was mostly parallel to the secondary (right) branch, resulting in the scour hole axis direction oriented to the secondary branch as well.

3.3 Morphology and evolution process

Figure 3 shows the evolution process of confluences B–F. Generally, the evolution trend of the overall braided pattern controlled the generation and disappearance of

Earth Surf. Dynam. Discuss., https://doi.org/10.5194/esurf-2018-85
Manuscript under review for journal Earth Surf. Dynam.
Discussion started: 18 December 2018

confluences. In 15 days the ridge between the two branches of confluence B was eroded away and the right branch grew to be the dominant one, with the main direction of flow and scour hole at the confluence switching from the left to the right branch (Figure 3b). Confluence C moved downstream to merge with its neighborhood pool (pool C') and became the deepest confluence, with its downstream channel (channel 1) becoming the largest channel in the river. Confluences D and F disappeared (Figure 3a), mainly due to the blockage of one of their branches. Confluence E shrank accompanied by a new confluence (confluence H) generation.

<Figure 3 insert here>

Figure 3 Evolution process of confluences B–F (erosion depth/m): (a) 3-D channel morphology; (b) 2-D plane map with depth-averaged velocity (m/s)

In particular, the significant growth of channel 1, closely related to the enlargement of confluence C, controlled the consequent evolution of downstream confluences, including D, E, F and H. In 15 days, confluence D gradually disappeared because the rapid growth of one of its branches —channel 1 promoted the blockage of the other branch. Due to the large amount of flow diverted into channel 1, confluence E and its branches experienced a decrease in flow, resulting in sediment deposition and overall confluence weakening. This also contributed to blocking branch 2 of confluence F, thereby leading to its ultimate disappearance. Meanwhile, as channel 1 grew, water overflowed out of its downstream channel bend, leading to the formation of a new channel (channel 3) and a new confluence (confluence H).

A remarkably steeper bed developed at the mouth of confluence branches, similar to avalanche faces in small-scale confluences. When one branch was obviously dominant, there was no visible avalanche face at its mouth, as shown by confluences B and F (Figure 3a), whose discharge ratios were 2.97 and 2.68, respectively (Table 2). Conversely, avalanche faces often existed in their secondary branch. However, when one branch did not fully dominate over the other one, avalanche faces generally occurred at both of the branch mouths. For example, at confluence E that exhibits two relatively equivalent branches in terms of discharge, there are two visible avalanche faces in front of the scour hole, with digging slopes being 1.624% for the left branch and 1.154% for the right branch, which are 70- and 50-folds of the original bed slope, respectively. Compared to small-scale confluences, the relatively gentle scour slopes observed in this study agreed with the findings of Szupiany et al. (2009) and Best and Ashworth (1997) in large sand-bed rivers.

A ridge sometimes developed in one branch of a confluence, which was often a newly formed branch that bifurcated from a channel bend. This typically happened in the early stage of confluence evolution. The ridge was initially located between two flow channels and as the new branch evolved, it was eroded away. Confluence B and the newly formed confluence H illustrate the process of ridge evolution, where the ridge can be viewed as a type of avalanche face.

4. Morphodynamic Processes at a Typical Confluence

Confluence E was chosen to perform an in-depth analysis of morphodynamic changes occurring at a typical confluence.

4.1 Evolution process

Figure 4 shows the evolution process of confluence E and its two branches. Confluence E experienced a period of expansion and then contraction from day 25 to 37, during which the dominant channel switched from the left to the right branch. The right branch began to lose its dominant role around day 32, as the left branch progressively increased in terms of size and discharge. Geometric changes in both branches through time illustrated that, the width of one channel declined along with the reduction in its flow discharge (Figure 6). As mentioned before, confluence E was ultimately largely filled with sediments due to flow recession as flow being diverted away from its upstream channel, when the right branch grew to play a dominant role.

<Figure 4 insert here>

Figure 4 Evolution process of confluence E (erosion depth/m)

Flow velocities at seven channel cross-sections on day 32 are shown in Figure 5, with five located on confluence E and two located on its two branches. Flow was more averagely distributed in the left branch than the right one. At the head of the confluence, section E3 exhibited two velocity cores, with a zone of lower velocity occurring in the central area where the two flows combined. At the immediately downstream section E4,

Earth Surf. Dynam. Discuss., https://doi.org/10.5194/esurf-2018-85
Manuscript under review for journal Earth Surf. Dynam.
Discussion started: 18 December 2018

flow concentrated and accelerated, with the two cores becoming indistinguishable. And at the subsequent section E5 where water was deepest, flow became even stronger with just one major core existing in the hole centre. Flow velocity at sections E4 and E5 peaked close to the right bank, promoting more sediments eroded away from the right bank and thus developing a steeper bank slope than the left one. Although water was deepest at section E5, which was approximately located in the center of the confluence, the fastest flow occurred at section E6, which was located toward the end of the confluence. A similar pattern was also often observed at the other six confluences shown in Figure 3. This might explain the commonly observed downstream migration of confluence scour holes, with deposition occurring at the hole heads due to upstream sediment deposition and erosion occurring at the hole tails due to contracted fast flow transporting sediments away. The flow in the two branches seemed to mingle faster than natural rivers (e.g. Szupiany et al., 2009), which might result from the rapid changing mixed bed layers in the model.

<Figure 5 insert here>

Figure 5 Distribution of depth-averaged flow velocities through confluence E on day 32 (erosion depth/m)

Sequential changes of flow discharge for the two branches converging at confluence E are illustrated in Figure 6. The left branch flow experienced a slight decrease and then steadily increased up to a maximum of 1092 m^3/s on day 33. This increase appeared to result partly from the disappearance of a middle channel between two adjacent bars enclosed by the left and right branches and partly from channel widening (Figure 4, day 25 to 32). Then the discharge gradually decreased down to 790 m^3/s till day 40. Meanwhile, discharge of the right branch increased up until day 26 due to channel constraint and the disappearance of a small bifurcation. After that, the sinuosity of the right branch bend increased, ultimately resulting in an avulsion, with the newly formed channel diverting a large portion of flow and consequently leading to a discharge decrease down to a minimum of 576 m^3/s. Between days 32 and 33 the two branches showed very similar discharge values. Before that the right branch was the dominant branch, while after that the left branch became dominant.

<Figure 6 insert here>

Figure 6 Sequential changes of flow discharge for the two branches of confluence E

4.2 Scour hole

A rapid displacement of the scour hole from the left to the right bank occurred (Figure 4), which was intricately linked to the evolution of the left and right branches. Specifically, the location of maximum erosion depth gradually moved from the left bank to the midchannel from day 25 to 32 when the discharge ratio between the two branches approached 1, and then migrated progressively closer to the right bank when the discharge ratio increased above 1. These movements of the scour hole in response to evolution of the two incoming flows further corroborate our previous observation that, confluence dynamics are largely controlled by upstream channel morphology and

Earth Surf. Dynam. Discuss., https://doi.org/10.5194/esurf-2018-85
Manuscript under review for journal Earth Surf. Dynam.
Discussion started: 18 December 2018

dynamics. Szupiany et al (2009) observed a similar process in field research, but they suggested that the velocity has the most significant influence other than the discharge ratio.

The orientation of the confluence angle was mainly controlled by the discharge of its two branches. Initially, the discharge of the right branch was substantially larger than that of the left branch (Figure 6) and the confluence axis aligned closely with the direction of the right branch. The orientation angles of the two branches were 28° and 4°, respectively (Figure 7). As discharge decreased in the right branch and increased in the left branch, the orientation angle of the right branch increased while the angle of the left branch decreased. By day 32, the two branches had comparable discharges and the scour axis approximately bisected the scour angle, with their orientation angles with respect to confluence E equal to 30.5° and 29.5°, respectively. As found in the experiment of Mosley (1976), the scour hole at confluence E enlarged and deepened considerably (Figure 4, day 32). The bed morphology of the confluence is related to a characteristic trough-shaped scour hole in the centre with a steeper front face than the tail, which has been observed in laboratory flumes by Ribeiro et al (2012).

< Figure 7 insert here>

Figure 7 Changes in the orientation angle of the two branches of confluence E with respect to the confluence axis

4.3 Relationships between flow velocity, shear stress and bed elevation

Simulation results for a cross-section on the left branch of confluence E (Figure 4,

Earth Surf. Dynam. Discuss., https://doi.org/10.5194/esurf-2018-85
Manuscript under review for journal Earth Surf. Dynam.
Discussion started: 18 December 2018

day 28) were extracted to analyse factors influencing morphodynamic changes in flow channel, with Figure 8 showing changes in flow velocity, shear stress and bed elevation across the section over eight days.

<Figure 8 insert here>

Figure 8 Spatial distribution of flow velocity, water depth and shear stress across the left branch of confluence E

Although the major peaks in flow velocity, shear stress and flow thalweg were initially located between the channel center and the right bank (peak 1 on day 15 in Figure 8), their exact locations differed, with the peak in flow thalweg being closer to the right bank. Over the next few days, shear stress and flow velocity continued to decrease until day 20, thereby promoting sediment deposition and river bed becoming shallower. The thalweg started to migrate by day 20 and was replaced by a newly grown one near the left bank by day 23. On the contrary, the secondary peak in shear stress close to the left bank (peak 2) continued to increase until it reached a value higher than peak 1 by day 20. But during this period bed topography remained nearly unchanged. As flow velocity increased in the left peak bank, shear stress reached its maximum value across the channel and more sediments were eroded and removed from the channel bed. Consequently, visible erosion occurred and river bed deepened near the left bank (Figure 8, day 23), forming a new thalweg in the channel, with peaks in flow velocity and shear stress occurring coincident to the thalweg. Generally, this process

Earth Surf. Dynam. Discuss., https://doi.org/10.5194/esurf-2018-85
Manuscript under review for journal Earth Surf. Dynam.
Discussion started: 18 December 2018

indicates that increasing shear stress and flow velocity caused local erosion, resulting in riverbed deepening. Importantly, there was a time lag before thalweg matched the peaks.

5. Conclusions

In the present study, an existing numerical model was employed to simulate natural large lowland braided rivers dominated by suspended sediment transport. The morphodynamic processes and their controlling factors at confluences were investigated and the following conclusions can be drawn.

1. In a braided river, a major change in the braiding pattern can affect the overall evolution process of the confluences downstream, e.g. confluence generation and enlargement, or decline and disappearance. Locally, flow from neighbouring upstream channels often plays a key role in influencing the dynamics and geometry of a confluence.

2. A steep bed slope similar to avalanche face in small-scale confluence can develop at the mouth of the confluent branches, with its formation being related to the degree of relative discharge dominance between the two branches. When one branch has a fully dominating discharge, an avalanche face only occurs at the mouth of the secondary branch; when the two branches have similar discharges, avalanche faces will occur at the mouths of both branches.

3. The confluence scour hole is normally located close to the bank of the secondary branch, which often has a steeper bank slope as the cross-sectional flow velocity peak usually occurs close to the bank of the secondary branch. Downstream migration of a

scour hole is common due to sediment deposition at its head and erosion at its tail, with maximum flow velocity occurring between the hole center and tail.

4. The discharge ratio between the two branches of a confluence controls its flow direction, shape, depth and orientation, which is also influenced by the upstream flow. As the discharge ratio decreases, the scour angle between the two branches enlarged and the scour hole deepens. The confluence flow direction and scour axis usually tends to be parallel to the dominant branch, and when the two branches become nearly equivalent, the scour axis approximately bisects the scour angle.

5. Increased shear stress and flow velocity may cause local erosion and scour deepening, when there is a time lag before the thalweg location coincides with the flow peaks.

Acknowledgements We are grateful for the financial support received from the Department of Science and Technology of the Guangdong Province (grant No. 2018A030310152), the National Natural Science Foundation of China (grant no. 41571172) and South China Agricultural University (grant No. 7600-218137).

Compliance with Ethical Standards.

Conflict of Interest None.

References

Ashmore, P.: Intensity and characteristic length of braided channel patterns, Canadian Journal of Civil Engineering, 36, 1656-1666, 2009.

Ashmore, P. and Parker, G.: Confluence scour in coarse braided streams, Water Resources Research, 19, 392-402, 1983.

Best, J. L.: The morphology of river channel confluences, Progress in Physical Geography, 10, 157-174, 1986.

Best, J. L.: Sediment transport and bed morphology at river channel confluences, Sedimentology, 35, 481-498, 1988.

Best, J. L. and Ashworth, P. J.: Scour in large braided rivers and the recognition of sequence stratigraphic boundaries, Nature, 387, 275-277, 1997.

Best, J. L. and Rhoads, B. L.: Sediment transport, bed morphology and the sedimentology of river channel confluences. In: River Confluences, Branches and the Fluvial Network, Rice, S. P., Roy, A., and Rhoads, B. L. (Eds.), Wiley-Interscience, Hoboken, New Jersey, United States, 45– 72, 2008.

Bolla Pittaluga, M., Repetto, R., and Tubino, M.: Channel bifurcation in braided rivers: Equilibrium configurations and stability, Water Resources Research, 39, 2003.

Ferguson, R. I., Ashmore, P. E., Ashworth, P. J., Paola, C., and Prestegaard, K. L.: Measurements in a Braided River chute and lobe: 1. Flow pattern, sediment transport, and channel change, Water Resources Research, 28, 1877-1886, 1992.

Gualtieri, C., Filizola, N., de Oliveira, M., Santos, A. M., and Ianniruberto, M.: A field study of the confluence between Negro and Solimoes Rivers. Part 1: Hydrodynamics and sediment transport, Comptes Rendus Geoscience, 350, 31-42, 2018.

Guillen-Ludena, S., Franca, M. J., Cardoso, A. H., and Schleiss, A. J.: Evolution of the hydromorphodynamics of mountain river confluences for varying discharge ratios and junction angles, Geomorphology, 255, 1-15, 2016.

Jang, C. L. and Shimizu, Y.: Numerical simulation of relatively wide, shallow channels with erodible banks, Journal of Hydraulic Engineering, 131, 565-575, 2005b.

Jang, C. L. and Shimizu, Y.: Numerical simulations of the behavior of alternate bars with different bank strengths, Journal of Hydraulic Research, 43, 596-612, 2005a.

Lin, B. L. and Falconer, R. A.: Hydrological and Environmental Modeling of Transport Processes in Rivers and Estuaries, Encyclopaedia of Hydrological Sciences, 1, 271-284, 2006.

Lin, B. L. and Falconer, R. A.: Tidal flow and transport modeling using ULTIMATE QUICKEST scheme, Journal of Hydraulic Engineering, 123, 303-314, 1997.

Nicholas, A. P.: Modelling the continuum of river channel patterns, Earth Surface Processes and Landforms, 38, 1187-1196, 2013.

Parsons, D. R., Best, J. L., Lane, S. N., Kostaschuk, R. A., Hardy, R. J., Orfeo, O., Amsler, M. L., and Szupiany, R. N.: Large river channel confluences. In: River Confluences, Tributaries and the Fluvial Network, Rice, S. P., Roy, A. G., and Rhoads, B. L. (Eds.), John Wiley & Sons, Ltd, Chichester, England, 73-91, 2008.

Preston, R. W.: The representation of dispersion in two-dimensional shallow water flow, Central Electricity Research Laboratories, Report No. TPRD/U278333/N84, 13pp, 1985.

Rhoads, B. L. and Kenworthy, S. T.: Flow structure at an asymmetrical stream confluence, Geomorphology, 11, 273-293, 1995.

Rhoads, B. L. and Kenworthy, S. T.: Time-averaged flow structure in the central region of a stream confluence, Earth Surface Processes and Landforms, 23, 171-191, 1998.

Rhoads, B. L., Riley, J. D., and Mayer, D. R.: Response of bed morphology and bed material texture to hydrological conditions at an asymmetrical stream confluence, Geomorphology, 109, 161-173, 2009.

Ribeiro, M. L., Blanckaert, K., Roy, A. G., and Schleiss, A. J.: Flow and sediment dynamics in channel confluences, Journal of Geophysical Research-Earth Surface, 117, 2012.

Riley, J. D., Rhoads, B. L., Parsons, D. R., and Johnson, K. K.: Influence of junction angle on three-dimensional flow structure and bed morphology at confluent meander bends during different hydrological conditions, Earth Surface Processes and Landforms, 40, 252-271, 2015.

Roy, N. and Sinha, R.: Understanding confluence dynamics in the alluvial Ganga–Ramganga valley, India: An integrated approach using geomorphology and hydrology, Geomorphology, 92, 182-197, 2007.

Schuurman, F. and Kleinhans, M. G.: Bar dynamics and bifurcation evolution in a modelled braided sand‐bed river, Earth Surface Processes and Landforms, 40, 1318–1333, 2015.

Schuurman, F., Marra, W. A., and Kleinhans, M. G.: Physics-based modeling of large braided sand-bed rivers: Bar pattern formation, dynamics, and sensitivity, Journal of Geophysical Research-Earth Surface, 118, 2509-2527, 2013.

Surian, N.: Fluvial Processes in Braided Rivers. In: Rivers—Physical, Fluvial and Environmental Processes, Rowiński, P. and Radecki-Pawlik, A. (Eds.), Springer

International Publishing, Switzerland, 402-425, 2015.

Szupiany, R. N., Amsler, M. L., Parsons, D. R., and Best, J. L.: Morphology, flow structure, and suspended bed sediment transport at two large braid-bar confluences, Water Resources Research, 45, W05415, 2009.

van Rijn, L. C.: Sediment transport, part II: Suspended load transport, Journal of Hydraulic Engineering, 110, 1613-1641, 1984.

Wei, Z.: A one dimensional sediment model for the Yellow River, Report of Wuhan University of Hydro-electrical Power (in Chinese), 1993.

Yang, H.: Development of a Physics-based Morphodynamic Model and its Application to Braided Rivers. PhD thesis, PhD thesis, Cardiff University, Cardiff, 235 pp., 2013.

Yang, H., Lin, B., Sun, J., and Huang, G.: Simulating Laboratory Braided Rivers with Bed-Load Sediment Transport, Water, 9, 2017.

Yang, H., Lin, B., and Zhou, J.: Avulsions in a Simulated Large Lowland Braided River, Water Resources Management, 32, 2301-2314, 2018.

Yang, H., Lin, B., and Zhou, J.: Physics‐based numerical modelling of large braided rivers dominated by suspended sediment, Hydrological Processes, 29, 1925-1941, 2015.

Zhou, J. and Lin, B.: Flow and sediment modelling. Beijing: China Hydropower Press, 173-278 (in Chinese), 2006.

Zhou, J., Lin, B., and Lin, B.: Rational Basis for Suspended Sediment Modeling, International Journal of Sediment Research, 18, 177-195, 2003.

Earth Surf. Dynam. Discuss., https://doi.org/10.5194/esurf-2018-85
Manuscript under review for journal Earth Surf. Dynam.
Discussion started: 18 December 2018

Figures 1-8

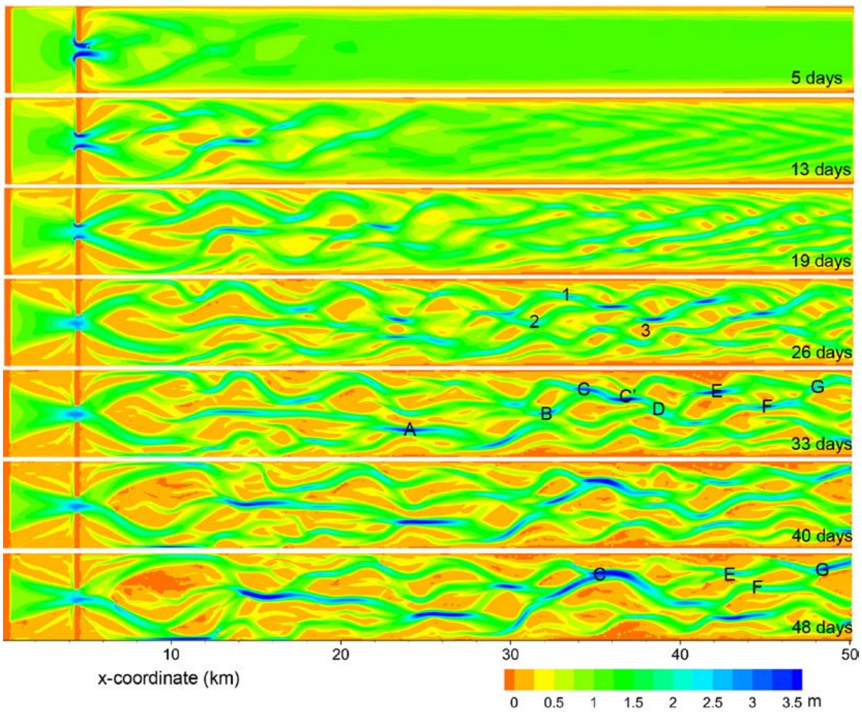

Figure 1 Sequential evolution of confluences in the modelled river (water depth/m)

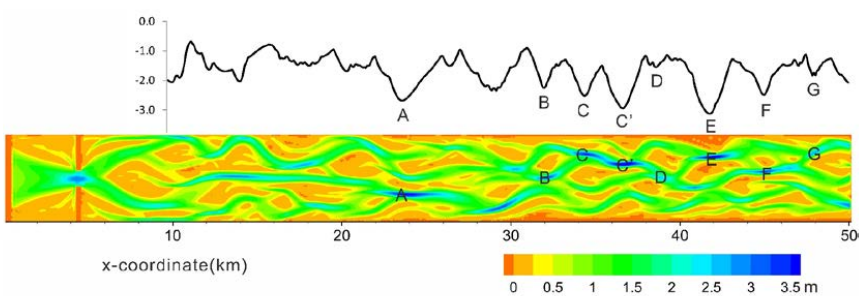

Figure 2 Cross-sectional maximum erosion depth compared to river geometry in a fully evolved river (day 33)

Earth Surf. Dynam. Discuss., https://doi.org/10.5194/esurf-2018-85
Manuscript under review for journal Earth Surf. Dynam.
Discussion started: 18 December 2018

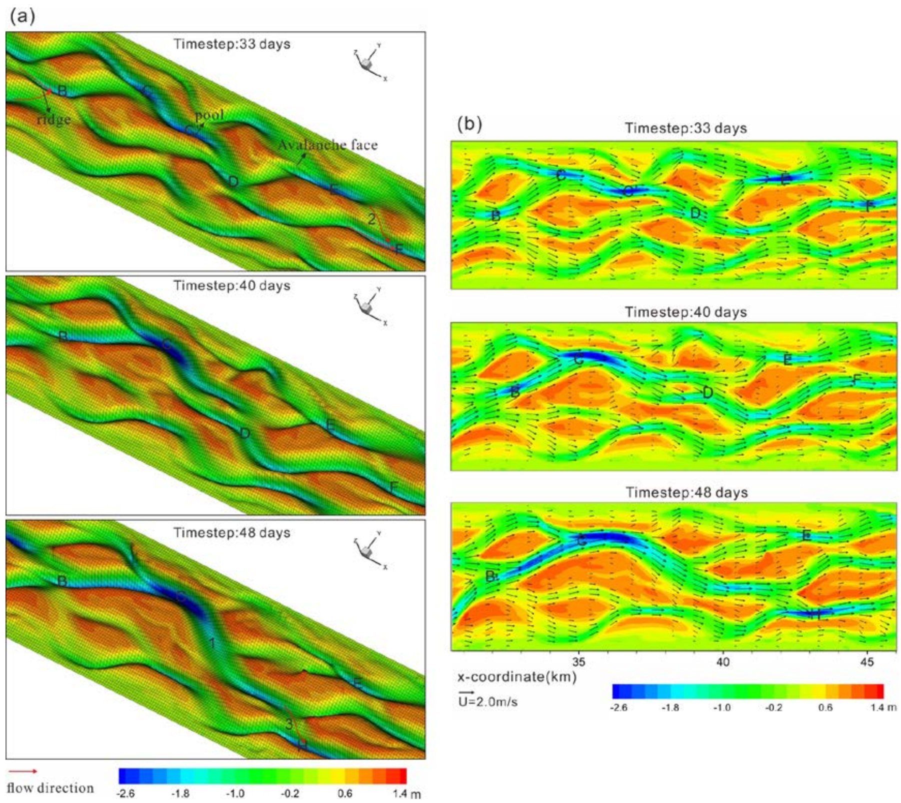

Figure 3 Evolution process of confluences B–F (erosion depth/m): (a) 3-D channel morphology; (b) 2-D plane map with depth-averaged velocity (m/s)

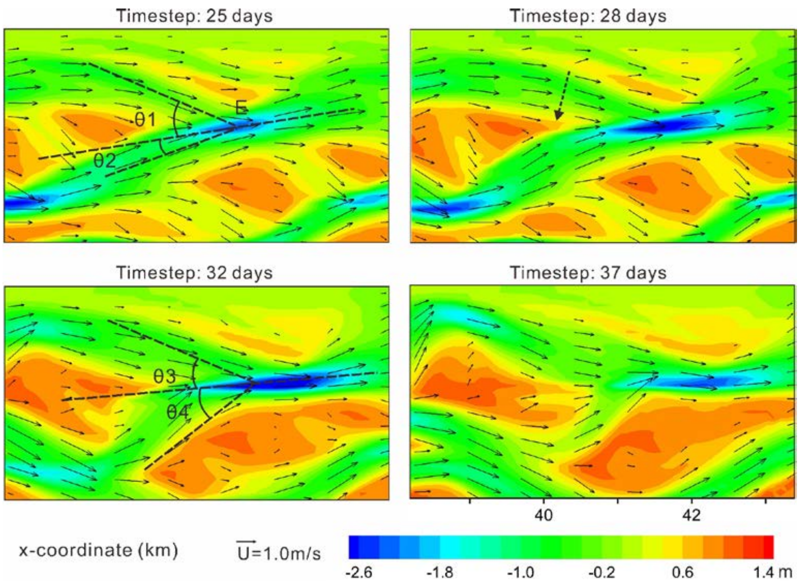

Figure 4 Evolution process of confluence E (erosion depth/m)

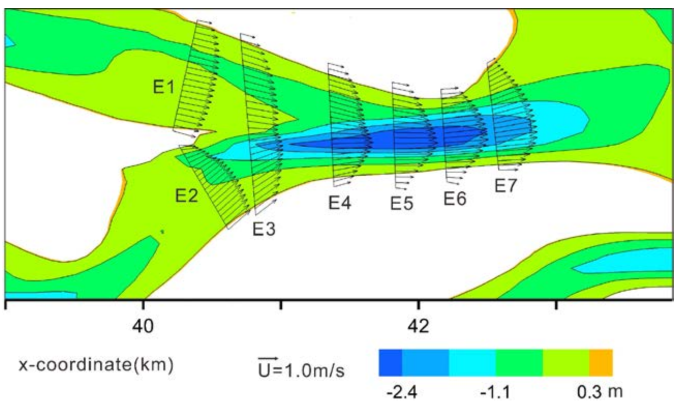

Figure 5 Distribution of depth-averaged flow velocities through confluence E on day 32 (erosion depth/m)

Earth Surf. Dynam. Discuss., https://doi.org/10.5194/esurf-2018-85
Manuscript under review for journal Earth Surf. Dynam.
Discussion started: 18 December 2018

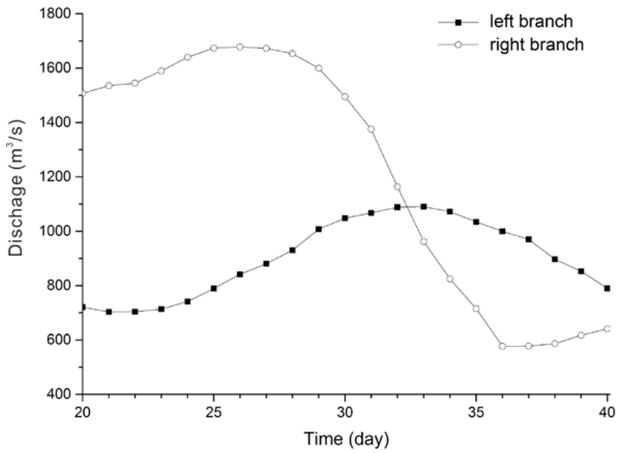

Figure 6 Sequential changes of flow discharge for the two branches of confluence E

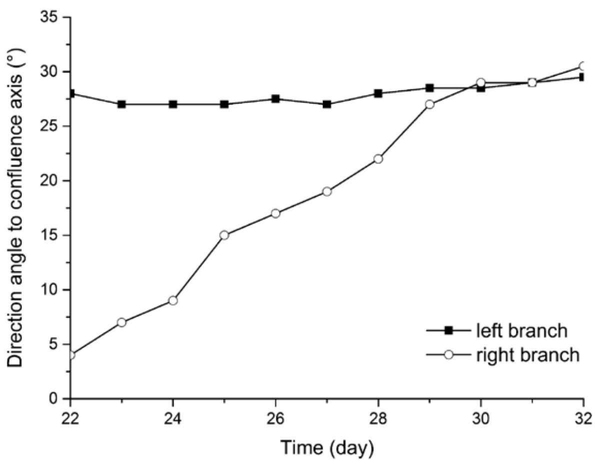

Figure 7 Changes in the orientation angle of the two branches of confluence E with respect to the confluence axis

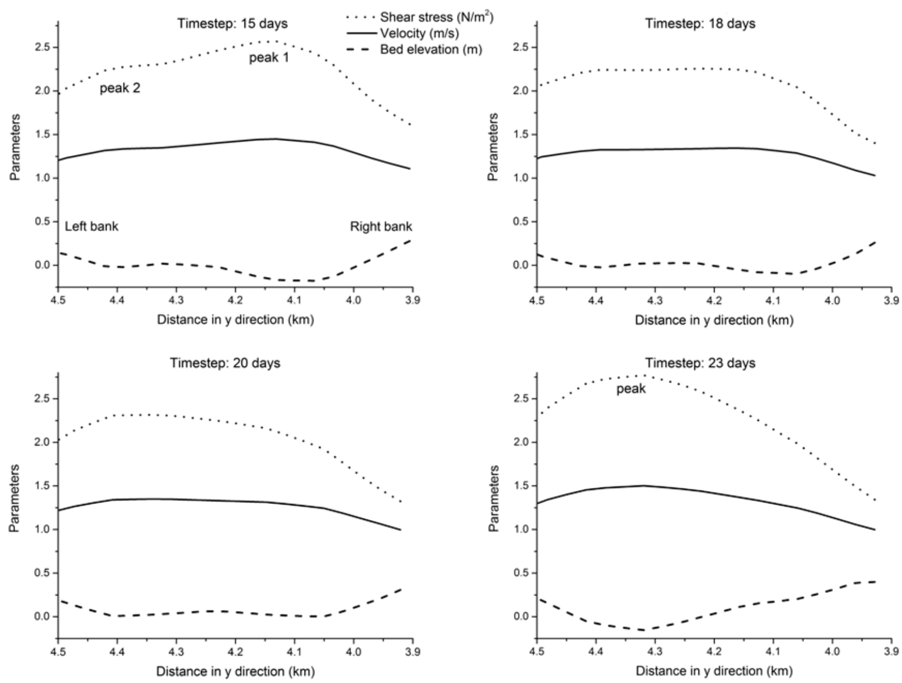

Figure 8 Spatial distribution of flow velocity, water depth and shear stress across the left branch of confluence E

Tables

Table 1 Parameters of seven typical confluences in a fully evolved river (day 33)

No.	Maximum scour depth (m)	Water depth (m)	maximum flow velocity (m/s)	Discharge of left branch (m^3/s)	Discharge of right branch (m^3/s)	Discharge ratio	Angle of two branches (°)	Angle to left branch (°)
A	-2.67	3.78	2.40	2133.1	652.4	3.27	34.22	8.10
B	-2.24	3.37	1.96	1599.3	539.3	2.97	34.68	15.55
C	-2.49	3.56	2.08	1385.0	1738.7	1.26	42.86	9.55
D	-1.51	2.58	1.73	1916.1	826.7	2.32	36.17	13.59
E	-3.10	3.99	2.12	1096.0	948.2	1.16	49.40	14.93
F	-2.46	3.42	2.10	498.3	1333.9	2.68	50.24	29.89
G	-2.31	3.27	2.08	1089.3	724.2	1.50	50.87	29.71

Note: Discharge ratio = discharge of dominant branch/discharge of secondary branch.